Sensors and Materials, Vol. 38, No. 6 (2026) 3033–3040
MYU Tokyo

S & M 4486

Thermoelectric Properties of N-type Low-temperature Thermoelectric Materials and Applications for Thermoelectric Sensors

Wen-Nan Wang, Pei-Yu Wang, and Tao-Hsing Chen*

Department of Mechanical Engineering, National Kaohsiung University of Science and Technology, No. 415, Jiangong Rd., Sanmin Dist., Kaohsiung City 807618, Taiwan.

(Received October 20, 2025; accepted December 26, 2025)

Keywords: thermoelectric materials, bismuth telluride, figure of merit, mechanical alloy

N-type $Bi_2Te_{3-x}Se_x$ (x = 0.3, 0.6, 0.7) thermoelectric materials and ball-milled N-type $Bi_2Te_{2.3}Se_{0.7}$ were prepared to investigate their thermoelectric properties. The effects of different processing methods on the crystal structure, thermoelectric properties, and microstructural morphology of N-type Bi_2Te_3 thermoelectric materials were investigated. X-ray diffraction analyses confirmed that all samples exhibited diffraction patterns consistent with the standard crystal structure. Electrical conductivity decreased with increasing temperature for all samples. Among them, the ball-milled sample exhibited the highest electrical conductivity of 233×10^3 $S \cdot m^{-1}$. Thermal conductivity reached its minimum at 310 K for all samples and increased thereafter with temperature. The ball-milled sample had the lowest thermal conductivity of 1.34 W/m·K. The figure of merit (*ZT)* increased with temperature for all samples. The ball-milled sample achieved the highest *ZT* of 0.132 at 400 K. It can be suitable for thermoelectric sensor applications.

1. Introduction

Since the industrial revolution, the global economy has developed rapidly, with countries heavily relying on nonrenewable energy sources such as coal, oil, and natural gas. However, the long-term excessive consumption of fossil fuels has led to increased carbon dioxide emissions, aggravating the greenhouse effect and air pollution, and making global warming increasingly severe. Although nuclear power generation technology is already mature, safety concerns such as the Chernobyl and Fukushima nuclear disasters still remain. Consequently, the international community has been actively seeking alternative energy sources in pursuit of sustainable energy and environmental protection.

Thermoelectric (TE) materials are capable of directly converting heat into electricity and vice versa through the thermoelectric effect.[1–3] They can be applied in thermoelectric generators and coolers, offering advantages such as no moving parts, noise-free operation, and simple structures.[4,5] Currently, TE materials have been widely applied in industrial waste heat

*Corresponding author: e-mail: thchen@nkust.edu.tw
https://doi.org/10.18494/SAM5987

ISSN 0914-4935 © MYU K.K.
https://myukk.org/

recovery, automotive exhaust energy utilization, aerospace technology, and wearable electronic devices. These applications help reduce energy waste and lower carbon emissions. The advancement of thermoelectric technology will further promote the application of renewable energy and contribute to achieving global carbon neutrality.[6–10]

The basic principle of the thermoelectric effect is that when a temperature gradient occurs within a material, electrons or holes move from the high-temperature region to the low-temperature region, generating an electric current or potential difference. Depending on the type of energy conversion, thermoelectric materials can be divided into power generation type and cooling type, suitable for different applications. With continuous technological progress, various high-efficiency TE materials have been developed. Among them, Bi_2Te_3-based thermoelectric materials have already been widely used in commercial thermoelectric modules.[11–13] However, TE materials still suffer from relatively low conversion efficiency, which limits their large-scale applications. Therefore, improving the performance of TE materials has become an important research topic. In this study, Bi_2Te_3 was selected as the base material. By adjusting the Se doping ratio and applying different processing methods, N-type bismuth telluride thermoelectric materials were synthesized.[14–16] The effects on their microstructure, Seebeck coefficient, thermal conductivity, electrical conductivity, and overall thermoelectric performance were systematically investigated. We hope to develop a novel and high-performance thermoelectric material for thermoelectric sensors.

2. Experimental Methods and Materials

In the first part of this study, the fabrication process was carried out using a vacuum induction melting (VIM) furnace. High-purity elemental blocks (purity > 99.99%) were melted at 650 °C for 10 min under vacuum. After cooling under vacuum for 30 min, ingots with a diameter of 15 mm and a thickness of 7–8 mm were obtained.

In the ball milling process, the high-purity alloy materials were ground into powders and then loaded into a planetary ball mill (JinKuo, F-P400) for ball milling at 350 rpm for 1 h. The milled powder slurry was dried using an evaporator at 45 °C under vacuum. The resulting ball-milled powders were subsequently placed in the VIM furnace, melted at 650 °C for 10 min, and cooled under vacuum for 30 min. Ingots with a diameter of 15 mm and a thickness of 7–8 mm were then obtained.

To verify the alloy composition and phase structure, the samples were first examined by energy-dispersive X-ray spectrometry (EDS) to confirm the added elements, followed by structural analysis using an X-ray diffraction (XRD) system. The microstructures of the materials were further observed by scanning electron microscopy (SEM). The ingot surfaces were polished to remove oxides, and the samples were cut into rectangular bars with dimensions of approximately $2 \times 2 \times 7$ mm^3 using a low-speed cutter for property measurements. Thermoelectric properties were characterized using a ZEM-3 system to measure the Seebeck coefficient, electrical conductivity, and power factor in the temperature range of 300–400 K. The thermal conductivity of the materials was measured using a physical property measurement system (PPMS) within the same temperature range.

3. Results and Discussion

3.1 XRD analysis

Figure 1 shows the XRD patterns of $Bi_2Te_{3-x}Se_x$ (x = 0.3, 0.6, 0.7, BM-0.7). Compared with the standard JCPDS, all N-type samples exhibited diffraction peaks consistent with the reference pattern, and no obvious impurity phases were detected. As the Se content increased from x = 0.3 to 0.7, the main diffraction peaks (0 1 5), (1 0 10), (1 1 0), and (2 0 5) shifted slightly toward higher 2θ values, indicating a reduction in lattice constant due to Te atoms being substituted by Se atoms. For the induction-melted samples, the diffraction peaks remained sharp and well-defined, suggesting an ordered layered crystal structure. In contrast, the ball-milled samples exhibited broader peaks with reduced intensity, implying smaller grain sizes and lower crystallinity, likely due to lattice defects.

3.2 Conductivity analysis

Conductivity was measured using the ZEM-3 system. To match the PPMS thermal conductivity measurements, the temperature range was set between 300 and 400 K, with data points collected at 10 K intervals.

As shown in Fig. 2, all samples exhibit decreasing electrical conductivity with increasing temperature, characteristic of degenerate semiconductors. Among the bulk samples, the Se-doped composition at x = 0.7 achieved the highest conductivity at 199 × 10^3 S·m^{-1} at 300 K, suggesting that a higher Se doping level at room temperature improves crystal structure and carrier concentration. However, as the temperature increased, the sample with x = 0.3 showed a slower decline in conductivity and maintained higher values than that with x = 0.7, indicating that a lower Se content provided a higher stability. Sun *et al.* also reported that in N-type $Bi_2Te_{3-x}Se_x$, Te or Se atoms may occupy Bi sites (forming Te–Bi or Se–Bi defects).[17] At higher Se doping levels, fewer Te–Bi pairs exist, leading to a decrease in carrier concentration.

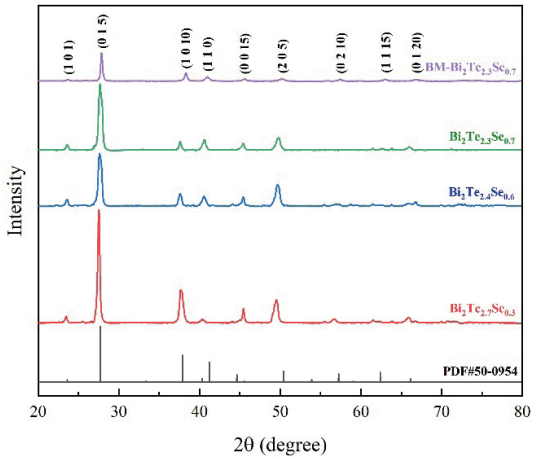

Fig. 1. (Color online) XRD patterns of $Bi_2Te_{3-x}Se_x$ (x = 0.3, 0.6, 0.7, BM-0.7)

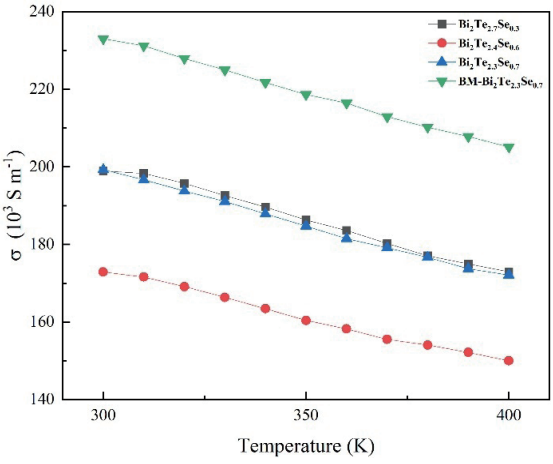

Fig. 2. (Color online) Relationship of conductivity and temperature for N-type $Bi_2Te_{3-x}Se_x$ (x = 0.3, 0.6, 0.7, BM-0.7).

The ball-milled $Bi_2Te_{2.3}Se_{0.7}$ sample showed a significantly higher conductivity than its bulk counterpart, with a maximum of 233×10^3 S·m^{-1} at 300 K. Even at 400 K, it maintained superior conductivity with a slower decreasing trend. This improvement is attributed to enhanced mixing and grain refinement during ball milling, which increases defect concentration, thereby boosting carrier concentration and electrical conductivity.

3.3 Seebeck coefficient analysis

Figure 3 shows the Seebeck coefficients of $Bi_2Te_{3-x}Se_x$ (x = 0.3, 0.6, 0.7, BM-0.7).[18] All samples exhibit negative values, confirming that they are N-type materials with electrons as dominant carriers. The Seebeck coefficients of all samples increase with temperature. Among the bulk samples, the composition with x = 0.3 achieved the highest absolute Seebeck coefficient of 39 μV/K at 400 K. As the Se content increased to x = 0.7, the overall Seebeck coefficient decreased, likely due to the inverse relationship between Seebeck coefficient and carrier concentration. The ball-milled $Bi_2Te_{2.3}Se_{0.7}$ sample displayed a much higher Seebeck coefficient than its bulk counterpart, reaching 52 μV/K at 400 K. This improvement is attributed to grain refinement caused by ball milling, which increases grain boundary density and enhances energy filtering at grain boundaries, thereby boosting the Seebeck coefficient.

$$S = \frac{\Delta V}{\Delta T} \tag{1}$$

3.4 Power factor analysis

Figure 4 presents the power factors [see Eq. (1)] of $Bi_2Te_{3-x}Se_x$ (x = 0.3, 0.6, 0.7, BM-0.7).[19] For the bulk samples, the power factor increased with temperature. Among them, $Bi_2Te_{2.7}Se_{0.3}$ exhibited the highest power factor, reaching approximately 2.6×10^{-4} W/m·K^2 at 400 K. This superior performance is attributed to its relatively high electrical conductivity and favorable Seebeck coefficient. In contrast, the x = 0.7 sample showed the lowest power factor due to its

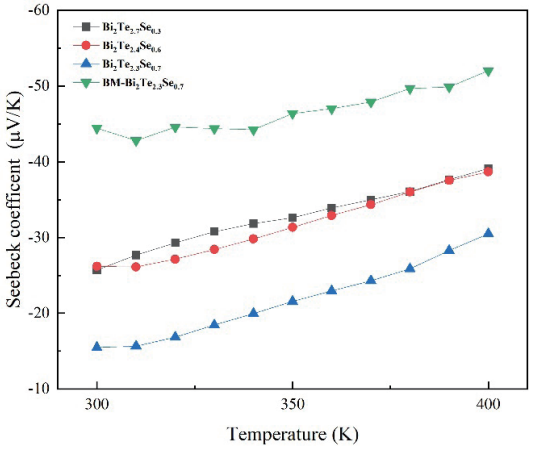

Fig. 3. (Color online) Seebeck coefficient versus temperature for n-type $Bi_2Te_{3-x}Se_x$ (x = 0.3, 0.6, 0.7, BM-0.7).

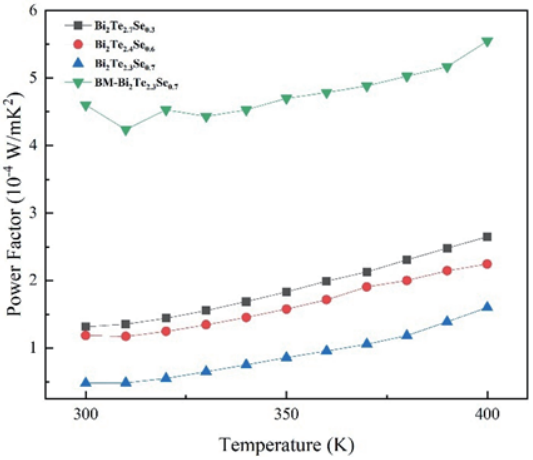

Fig. 4. (Color online) Power factor versus temperature for n-type $Bi_2Te_{3-x}Se_x$ (x = 0.3, 0.6, 0.7, BM-0.7).

significantly reduced Seebeck coefficient. The ball-milled $Bi_2Te_{2.3}Se_{0.7}$ sample demonstrated a substantial improvement in power factor compared with its bulk counterpart, maintaining higher values across the entire temperature range. At 400 K, it reached a maximum of 5.6×10^{-4} W/m·K². This enhancement primarily results from microstructural modifications introduced by ball milling, including increased number of grain boundaries and defect density, which improved performance without significantly reducing electrical conductivity.

$$PF = S^2\sigma, \tag{2}$$

where σ is the electrical conductivity.

3.5 Thermal conductivity analysis

Figure 5 shows the thermal conductivity of $Bi_2Te_{3-x}Se_x$ (x = 0.3, 0.6, 0.7, BM-0.7). In all samples, the thermal conductivity increased with temperature. Among the bulk samples, $Bi_2Te_{2.3}Se_{0.7}$ had the highest value of 2.46 W/m·K at 400 K, whereas $Bi_2Te_{2.7}Se_{0.3}$ exhibited the lowest thermal conductivity of 1.48 W/m·K at 310 K. The higher conductivity of x = 0.7 is attributed to its larger grain size and fewer grain boundaries, which reduce phonon scattering and thus limit the suppression of lattice thermal conductivity. In contrast, the ball-milled $Bi_2Te_{2.3}Se_{0.7}$ sample exhibited a significantly lower thermal conductivity than its bulk counterpart, remaining below all bulk samples across the entire temperature range. It achieved the lowest thermal conductivity of 1.34 W/m·K at 310 K, confirming that grain refinement and increased grain boundary scattering caused by ball milling effectively reduced lattice thermal conductivity.

3.6 Figure of merit (*ZT*)

Figure 6 shows the dimensionless ZT [see Eq. (2)] for $Bi_2Te_{3-x}Se_x$ (x = 0.3, 0.6, 0.7, BM-0.7).[20–22] For all samples, ZT increased with temperature. Among the bulk samples, $Bi_2Te_{2.7}Se_{0.3}$ achieved

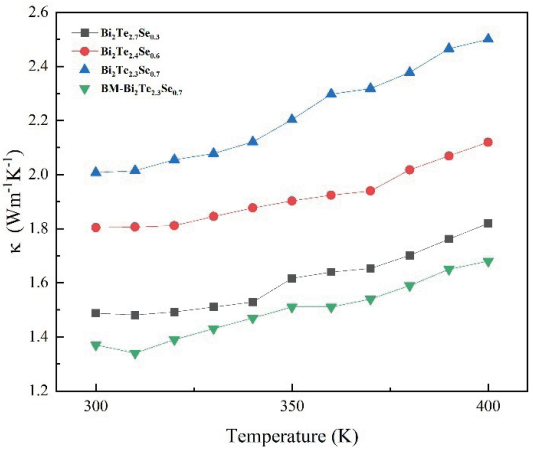

Fig. 5. (Color online) Thermal conductivity versus temperature for n-type $Bi_2Te_{3-x}Se_x$ (x = 0.3, 0.6, 0.7, BM-0.7).

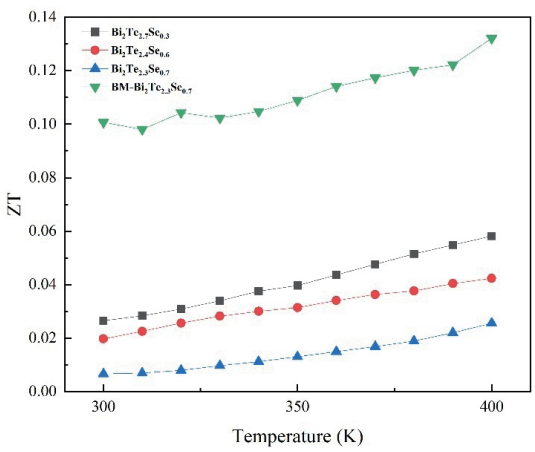

Fig. 6. (Color online) ZT versus temperature for n-type $Bi_2Te_{3-x}Se_x$ (x = 0.3, 0.6, 0.7, BM-0.7).

the highest *ZT* of 0.058 at 400 K, owing to its relatively high electrical conductivity, favorable Seebeck coefficient, and lowest thermal conductivity. In contrast, $Bi_2Te_{2.3}Se_{0.7}$ showed the poorest performance, as its low Seebeck coefficient and high thermal conductivity offset its good electrical conductivity. The ball-milled $Bi_2Te_{2.3}Se_{0.7}$ sample exhibited a significantly higher *ZT* than the bulk counterpart, reaching a maximum of 0.132 at 400 K and maintaining a *ZT* of 0.1 even at 300 K. This result indicates that ball milling refined the grains, allowing the sample to achieve high electrical conductivity and Seebeck coefficient while maintaining low thermal conductivity, thereby enhancing the overall thermoelectric performance.

$$Z\,T = S^2 \cdot \sigma \cdot T \cdot \kappa^{-1}, \tag{3}$$

where σ is the electrical conductivity and κ is the thermal conductivity.

4. Conclusions

In this study, bulk N-type $Bi_2Te_{3-x}Se_x$ (x = 0.3, 0.6, 0.7) samples and a ball-milled $Bi_2Te_{2.3}Se_{0.7}$ sample were fabricated using a vacuum induction melting furnace. The phase structures, surface morphologies, thermoelectric properties, and *ZT* values of the specimens were systematically investigated. On the basis of the results, the following conclusions can be drawn:

1. XRD and SEM analyses confirmed that all specimens exhibited diffraction patterns consistent with the standard reference card. SEM images revealed that all samples had typical layered structures, with the ball-milled sample showing the densest morphology.
2. Electrical conductivity decreased with increasing temperature for all samples. Among them, the ball-milled sample exhibited the highest electrical conductivity of 233×10^3 S·m^{-1}.
3. The Seebeck coefficient increased with temperature for all the samples. The ball-milled sample achieved the highest Seebeck coefficient of 52 μV/K.
4. Thermal conductivity reached its minimum at 310 K for all samples and increased thereafter with temperature. The ball-milled sample had the lowest thermal conductivity of 1.34 W/m·K.
5. *ZT* increased with temperature for all samples. The ball-milled sample achieved the highest *ZT* of 0.132 at 400 K.

Acknowledgments

This paper was finished through Research Project NSTC 114-2637-E-992-004, which is supported by the National Science and Technology Council of Taiwan. The authors would like to express their gratitude to the National Science and Technology Council for its support, which enabled the smooth completion of this research. The authors also gratefully acknowledge the use of EM000700 and XRD003100 of NSTC 114-2740-M-006-001, which belong to the Core Facility Center of National Cheng Kung University.

References

1 M. Brignone and A. Ziggiotti: AIP Conf. Proc. **1449** (2012) 493. https://doi.org/10.1063/1.4731601
2 K. Kawajiri, Y. Kishita, and Y. Shinohara: Sustainability **13** (2021) 13630. https://doi.org/10.3390/su132413630
3 K. Gaurav and S. K. Pandey: J. Renewable Sustainable Energy **9** (2017) 014701. https://doi.org/10.1063/1.4976125
4 J. Yang and T. Caillat: MRS bulletin **31** (2006) 224. https://doi.org/10.1557/mrs2006.49
5 D. Crane, B. Poudel, W. Li, and G Joshi: MRS Bulletin **50** (2025) 902. https://doi.org/10.1557/s43577-025-00946-3
6 T. H. Chen, S. A. Tsai, and T. Y. Zeng: Sens. Mater. **29** (2017) 1637. https://doi.org/10.18494/SAM.2017.1737
7 T. H. Chen and M. T. Hong: Sens. Mater. **28** (2017) 503. https://doi.org/10.18494/SAM.2016.1306
8 J. He and T. M. Tritt: Science **357** (2017) eaak9997. https://doi.org/10.1126/science.aak9997
9 X. L. Shi, J. Zou, and Z. G. Chen: Chem. Rev. **120** (2020) 7399. https://doi.org/10.1021/acs.chemrev.0c00026
10 Y. Pei, H. Wang, and G. J. Snyder: Adv. Mater. **24** (2012) 6125. https://doi.org/10.1002/adma.201202919
11 J. Pei, B. Cai, H. L. Zhuang, and J. F. Li: Natl. Sci. Rev. **7** (2020) 1856. https://doi.org/10.1093/nsr/nwaa259
12 S. E. Yang, H. Han, and J. S. Son: J. Phys-Energy **6** (2024) 022003. https://10.1088/2515-7655/ad3983
13 X. H. Ji, X. B. Zhao, Y. H. Zhang, B. H. Lu, and H. L. Ni: J. Alloy Compd. **387** (2005) 282. https://doi.org/10.1016/j.jallcom.2004.06.047
14 Y. Saberi and S. A. Sajjadi: J. Alloy Compd. **904** (2022) 163918. https://doi.org/10.1016/j.jallcom.2022.163918Get rights and content
15 S. Bano, A. Kumar, B. Govind, A. H. Khan, A. Ashok, and D. K. Misra: J. Mater. Sci.: Mater. Electron. **31** (2020) 8607. https://doi.org/10.1007/s10854-020-03396-6
16 M. Liu, X. Zhang, S. Zhang, and Y. Pei: Nat. Commun. **15** (2024) 6580. https://doi.org/10.1038/s41467-024-50898-6
17 J. Sun, Z. Shu, J. Yang, T. Wang, B. Zhu, and J. He: J. Appl. Phys. **130** (2021) 135103. https://doi.org/10.1038/nmat1821
18 V. Zlatic and R. Monnier: Modern Theory of Thermoelectricity (OUP Oxford, 2014) pp. 19–21.
19 A. M. Dehkordi, M. Zebarjadi, J. He, and T. M. Tritt: Mater. Sci. Eng.: R: Rep. **97** (2015) 1. https://doi.org/10.1016/j.mser.2015.08.001
20 H. Ohta, S.Kim, Y. Mune, T. Mizoguchi, K. Nomura, S. Ohta, T. Nomura, Y. Nakanish, Y. Ikuhara, M. Hirano, H. Hosono, and K. Koumoto: Nat. Mater. **6** (2007) 129. https://doi.org/10.1038/nmat1821
21 J. Martin: Meas. Sci. Technol. **24** (2013) 085601. https://doi.org/10.1088/0957-0233/24/8/085601
22 J. de Boor, C. Stiewe, P. Ziolkowski, T. Dasgupta, G. Karpinski, E. Lenz, F. Edler, and E. Mueller: J. Electron. Mater. **42** (2013) 1711. https://doi.org/10.1007/s11664-012-2404-z

About the Authors

Wen-Nan Wan received his M.S. degree from Chi-Yi University, Taiwan, in 2022. He is now a Ph.D. student in the Department of Mechanical Engineering, National Kaohsiung University of Science and Technology. Since 2010, he has been the general manager of SHIEH HO TIEN ENTERPRISE Co., LTD. His research interests are in optical materials, heat transfer, fluid sensors, and pressure sensors.

Pei-Yu Wang received her B.S. degree from National Kaohsiung University of Science and Technology, Taiwan, where she is currently studying for her M.S. degree. Her research interests are in thermoelectric materials, materials engineering, and sensors.

Tao-Hsing Chen received his B.S. degree from National Cheng Kung University, Taiwan, in 1999 and his M.S. and Ph.D. degrees from the Department of Mechanical Engineering, National Cheng Kung University, in 2001 and 2008, respectively. From August 2008 to July 2010, he was a postdoctoral researcher at the Center for Micro/Nano Science and Technology, National Cheng Kung University. In August 2010, he became an assistant professor at National Kaohsiung University of Applied Sciences (renamed National Kaohsiung University of Science and Technology), Taiwan. Since 2016, he has been a professor at National Kaohsiung University of Science and Technology. His research interests are in metal materials, TCO thin films, thermal sensors, and photosensors. (thchen@nkust.edu.tw)